We are IntechOpen,
the world's leading publisher of
Open Access books
Built by scientists, for scientists

## 4,800
Open access books available

## 122,000
International authors and editors

## 135M
Downloads

Our authors are among the

## 154
Countries delivered to

## TOP 1%
most cited scientists

## 12.2%
Contributors from top 500 universities

**WEB OF SCIENCE**™

Selection of our books indexed in the Book Citation Index
in Web of Science™ Core Collection (BKCI)

Interested in publishing with us?
Contact book.department@intechopen.com

Numbers displayed above are based on latest data collected.
For more information visit www.intechopen.com

# Phase Transitions, Dielectric and Ferroelectric Properties of Lead-free NBT-BT Thin Films

N. D. Scarisoreanu, R. Birjega, A. Andrei, M. Dinescu, F. Craciun and C. Galassi

Additional information is available at the end of the chapter

## 1. Introduction

Ferroelectric perovskites based on $Na_{0.5}Bi_{0.5}TiO_3$ (NBT) are considered among the most promising lead-free candidate materials to substitute $Pb(Zr_{1-x}Ti_x)O_3$ (PZT) in devices designed to respect standards and environmental laws. Taking into account the toxicity of lead-based systems, there are numerous lead-free piezoelectric materials under investigation in worldwide spread laboratories for replacing PZT in future devices. Constant efforts are made to find viable replacements for all these materials containing harmful elements.

Solid-solution systems based on lead-free perovskites like $Na_{0.5}K_{0.5}NbO_3$ (NKN), $BaTiO_3$ (BT), $Na_{0.5}Bi_{0.5}TiO_3$ (NBT) or bismuth layered-structured $SrBi_2Ta_2O_9$ (SBT), and $SrBi_2Nb_2O_9$ (SBN) are considered as viable alternatives for replacing lead-based materials. For example, $(K,Na)NbO_3$–$LiTaO_3$–$LiSbO_3$ alkaline niobate ceramics exhibit a $d_{33}$ piezoelectric coefficient up to 416 pC/N together with Curie temperature $T_c$ around 526 K, as reported by Saito *et al* [1]. Sodium/bismuth titanate (NBT) belongs to the bismuth-based perovskites in which the A-site atom is replaced. The crystalline structure, phase transitions and physical properties have been intensively studied since the discovery of the material in 1960 by Smolensky *et al* [2]. NBT has a relatively high depolarization temperature, $T_d$ = 470 K, high remanent polarization, 38 $\mu C/cm^2$ and piezoelectric coefficient $d_{33}$ = 125 pC/N [3]. However, owing to the high value of the coercive field and high electrical conductivity, NBT cannot be easily polarized, therefore different A-site substitutions have been attempted to avoid this drawback.
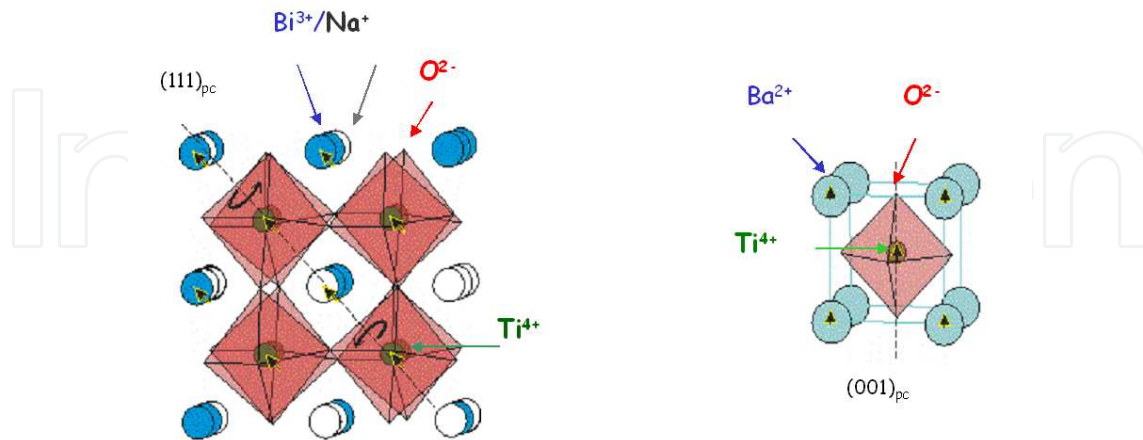
**Figure 1.** The end-members of perovskite NBT-BT: rhombohedral NBT and tetragonal BT. Cations $Na^+/Bi^{3+}$ and $Ba^{2+}$ occupy the A-sites while $Ti^{4+}$ occupies B-sites (oxygen octahedra centers).

The solid solution with $BaTiO_3$, (1-x) NBT-x BT shows a morphotropic phase boundary (MPB) between the rhombohedral and the tetragonal phase, at x between 0.06 and 0.07 for which the material properties are considerably improved. Indeed $d_{33}$ values up to 450 pC/N, and huge electric field-induced strain have been reported [4, 5]. Figure 1 shows the crystalline structures of the NBT and BT end members at room temperature. Perovskite structure deformations include oxygen octahedral rotations around different axis and cation shifts, therefore giving rise to a complex succession of ferroelastic and ferroelectric phase transformations with temperature variation.

Due to this polymorphic structure, NBT and NBT-BT have been also intensively studied in order to clarify their complicated phase transitions, which still pose questions [6].Structural and polar transformations in NBT-BT are more complicated than in other perovskite solid solutions, also due to the strong disorder of the A-sites occupied by $Na^+$, $Bi^{3+}$ or $Ba^{2+}$ ions, with different valence, mass and ionic radius. NBT transforms successively, from the high temperature cubic paraelectric into tetragonal antiferroelectric (or ferrielectric) and further into a rhombohedral ferroelectric phase [6]. In solid solution with BT, the ground ferroelectric phase changes from rhombohedral *R3c* to tetragonal ferroelectric *P4mm*, at the so-called morphotropic phase boundary (MPB) ($x \approx 0.06$-$0.07$) [5, 7, 8]. The phase diagram of NBT-BT bulk material, mainly based on dielectric measurements, was completed by Cordero *et al* by performing direct anelastic measurements, the border between tetragonal and cubic phases being evidenced [9, 10, 11].

For NBT-BT thin films growth many techniques have been used. Guo *et al.* have investigated NBT-BT-based tri-layered films prepared by chemical solution deposition as a possible solu-

tion to the problem of avoiding leakage currents under high electric fields [12, 13]. Using pulsed laser deposition (PLD), Duclère *et al.* have reported the heteroepitaxial growth of NBT thin films on epitaxial platinum electrodes supported on a sapphire substrate [14]. More recently, M.Bousquet *et al* have described the electrical properties of (110)- oriented NBT thin films deposited by laser ablation on (110)Pt/(110) $SrTiO_3$ substrates [15]. They reported the coexistence of two kinds of grains with different shapes in the films, flat and elongated grains corresponding to (100) and (110) oriented NBT crystallites. The effects of Bi- excess in target on the dielectric and ferroelectric properties of the films have been also presented; the reported values for relative permittivity and remnant polarization were $\varepsilon_r \approx 225\text{-}410$ and 14 $\mu C/cm^2$, respectively. Furthermore, very recently, the electrical properties of (100)-oriented $Na_{0.5}Bi_{0.5}TiO_3\text{-}BiFeO_3$ thin films deposited by sol-gel have been reported by Qin et al, aiming to important applications such as photovoltaic devices [16].

However, despite the fact that ferroelectric materials with MPB have enhanced ferroelectric and piezoelectric properties, it is difficult to transpose them in thin films since MPB is limited to a small composition range. Almost all the physical parameters involved in thin films deposition like the substrate type, the microstructure and stress have strong impact on their physical properties [17]. In some previous papers we have investigated the role of different deposition parameters on NBT-BT film growth and properties [18, 19]. In this chapter, we discuss the role of certain experimental conditions like deposition temperature and substrate type, as well as of the amount of BT present in the target on crystalline structure, microstructure, dielectric properties, phase transition temperatures and stability limits of ferroelectric phases in NBT-BT thin films produced by PLD.

## 2. Experimental method

Pulsed laser deposition (PLD) was used for the film growth. The targets with composition $(NBT)_{1-x}(BT)_x$ ($x$ = 0.06-0.08), further called NBT-BT6 and NBT-BT8, have been prepared following the mixed oxide route and sintered at 1150 °C for 2 h. The sintering was performed in crucibles with the sample surrounded with NBT pack, in order to avoid the loss of Na and Bi, which occurs at temperatures over 1000 °C; more details can be found in Ref.11. X-ray diffraction analysis evidenced the obtaining of pure perovskite phase. The microstructure of the sintered targets was investigated on polished and etched surfaces by scanning electron microscopy. The observed grain sizes were 2-10 μm.

For the film deposition, a Surelite II Nd:YAG pulsed laser with wavelength of 265 nm, pulse duration of 5 ns and frequency 10 Hz, has been employed. The laser fluence was set at 1.6 $J/cm^2$. The films were grown on Nb:STO and $Pt/TiO_2/SiO_2/Si$ substrates, placed at a distance of about 4.3 cm from the target. Different sets of films have been grown at different substrate temperatures, ranging between 650-730 °C. Deposition and after-deposition cooling were performed in flowing oxygen atmosphere (0.3-0.6 mbar) to favour the formation of perovskite phase without oxygen vacancies. Chemical composition was checked via SIMS technique using a Hiden SIMS/SNMS system. The thickness of the thin films, evaluated by spectroellipsometry, was between 300-500 nm.

For the investigation of the crystalline structure of the targets and films, a PANalytical X'pert MRD diffractometer in Bragg-Brentano geometry was used. The measurements were performed with a step size of $0.02^0$ and with a scanning time on step of 25 s or 250 s, depending on the angular range.

The film surface morphology was examined by AFM (model XE100, Park Systems). Piezoelectric force microscopy measurements were performed with a PFM system which includes a lock-in amplifier SR-830 and a dc- high voltage amplifier WMA-280. Conductive all-metal Pt tips were employed for these measurements were the switching characteristcs of the films have been tested.

Several Au electrode dots with an area of about 0.22 mm² have been evaporated through a mask on the films for electrical characterization. Polarization hysteresis was measured by using a Radiant Technology RT66A ferroelectric test system, in the virtual ground mode. The dielectric measurements were carried out in a frequency range between 200 Hz and 1 MHz using an HP 4194A impedance analyzer and an HP 4284A LCR meter with a four wire probe. The measurements were performed at 1.5 K/min between 300 and 570 K in a Delta Design climatic chamber model 9023 A (on targets) and in a Linkam variable-temperature stage (model HFS 600E) on films.

## 3. Results and discussion.

### 3.1. Growth mode of NBT-BT thin films.

The microstructure of ceramic thin films is one of the most important factors that influence their physical properties. Since the growth mode of thin films is strongly dependent on the substrate type, we investigated the deposition of NBT-BT thin films on two different types of substrates:

1.   single crystal $SrTiO_3$: Nb (Nb:STO) and

2.   $Pt/TiO_2/SiO_2/Si$.

The AFM pictures obtained on the two sets of films show important microstructural differences, mainly due to different growth mechanisms. In Figure 2 we show AFM images taken on a NBT-BT6 film deposited on Nb: STO monocrystalline substrate at 650 $^0$C. It can be observed that a first stage of growth resulting into a continuous layer stops when the critical thickness for misfit dislocations (probably a few tens of nm) is reached. After that, the growth continues in platelet-like form (see details in Fig. 2 b). If the deposition temperature is not sufficiently high to favor material exchange between platelets via surface migration, successive layers will grow on the top of the first islands and the growth will result into a discontinuous layer. This explains the platelet-like aspect of the film shown in Figure 2.
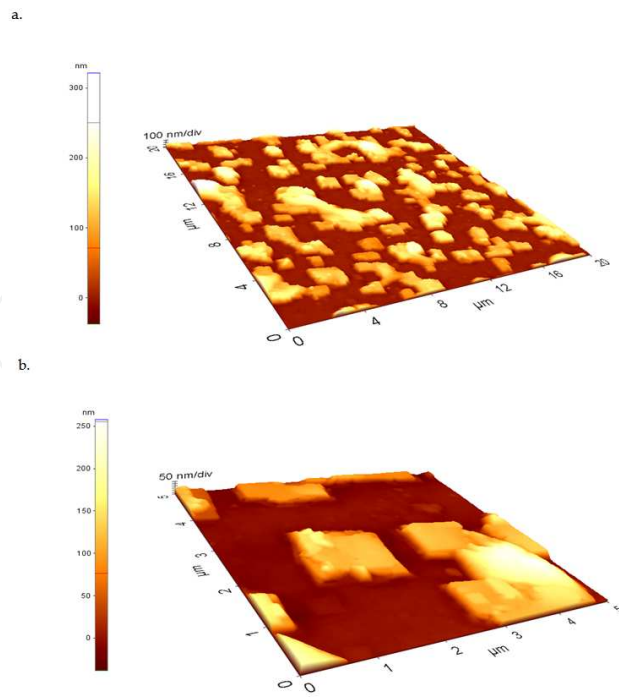
**Figure 2.** AFM images of NBT-BT6% films deposited on Nb:STO substrates at temperature of 650 °C. The displayed surfaces are 20x20 μm² (a) and 5x5 μm² (b).
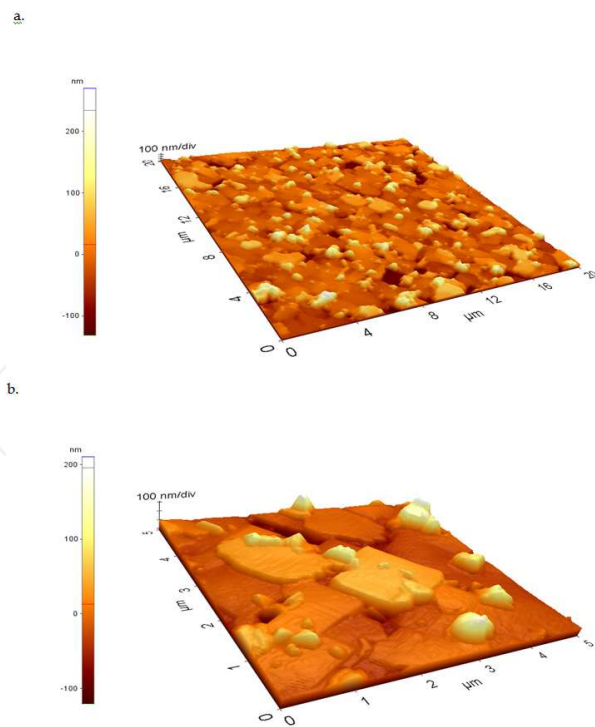


**Figure 3.** AFM images of NBT-BT6% films deposited on Nb:STO substrates at 700°C. The displayed surfaces are 20x20 μm² (a) and 5x5 μm² (b).

However, raising the substrate temperature to 700 $^0$C during the deposition of a second set of films while keeping constant all the other parameters, including the number of laser pulses, produces a uniform layer of continuous platelets, on top of which new islands nucleate (Figure. 3).

A rather different morphology is displayed by NBT-BT films grown on Pt/TiO$_2$/SiO$_2$/Si (Fig. 4 and 5). In this case, the growth progresses from the beginning in island-like form since the polycrystalline Pt layer provide the nucleation sites for their formation. Moreover, these NBT-BT islands grow on the Pt layer without preserving a unique orientation, due to the same reason. Instead films grown on Nb:STO monocrystalline structures are uniaxially (001)-oriented, as it will be shown in the next section.
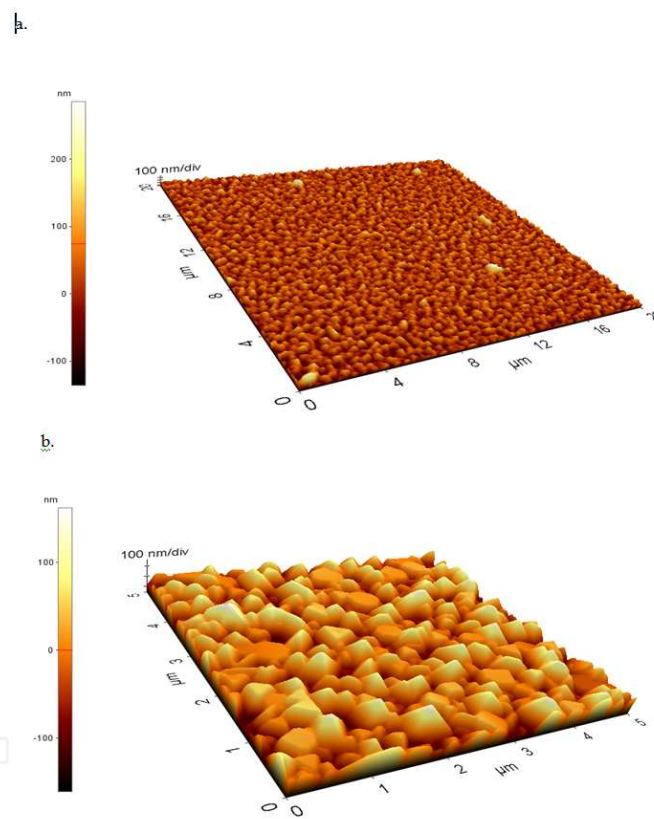


**Figure 4.** AFM images of NBT-BT6% films deposited on Pt/TiO$_2$/SiO$_2$/Si substrate at a temperature of 700 $^o$C. The displayed surfaces are 20x20 μm$^2$ (a) and 5x5 μm$^2$ (b).

A fine microstructure with grain size ranging from a few tens of nm up to a few hundred of nm is displayed by NBT-BT6 films (Fig. 4). We note the striking difference with bulk samples microstructures (not shown here), which consists of crystallites of 1-10 μm size.

A similar fine microstructure is displayed by NBT-BT8% films grown on Pt/TiO$_2$/SiO$_2$/Si (Fig. 5 a). However, the enlarged AFM image displayed in Fig 5 b) reveales a somewhat different aspect with triangular nanograins lying in plane.
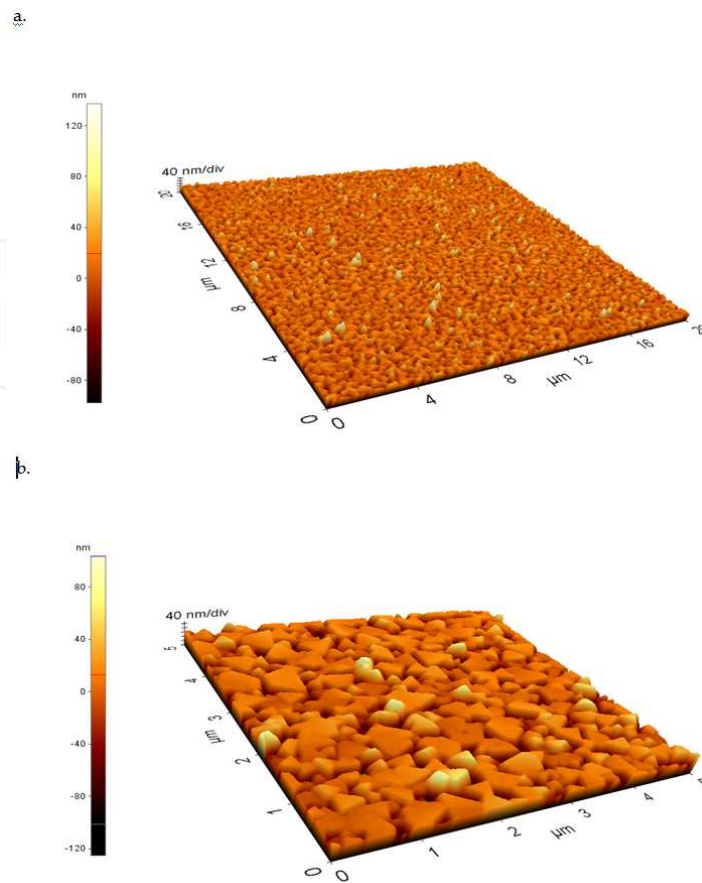
a.

b.

**Figure 5.** AFM images of NBT-BT8% films deposited on Pt/TiO$_2$/SiO$_2$/Si substrate at a temperature of 700 $^\circ$ C. The displayed surfaces are 20x20 µm$^2$ (a) and 5x5 µm$^2$ (b).

### 3.2. Crystalline structure

The XRD spectrum of NBT-BT6 target corresponds to a mixture of rhombohedral R3c and tetragonal P4mm phases, as shown by the splitting of (111) and (200), (012) and (024) rhombohedral peaks in the bottom pattern in Fig. 6 [20]. The main Miller index of the rhombohedral phase are depicted horizontally on the bottom of the figures while those of the tetragonal phase vertically above. On the same graph, the pattern corresponding to the NBT-BT6 film grown on Pt/TiO$_2$/SiO$_2$/Si at 700 $^0$C is given. The curve corresponding to NBT-BT6/Pt/TiO$_2$/SiO$_2$/Si film deposited in the same conditions but at a substrate temperature of 650$^0$ exhibits similar features as we had reported and is not presented here [18].The as deposited thin films exhibit pure perovskite phase with symmetry congruent with that of the target. The reflection peaks indicate a randomly oriented structure, consistent with the polycrystalline nature of the films.
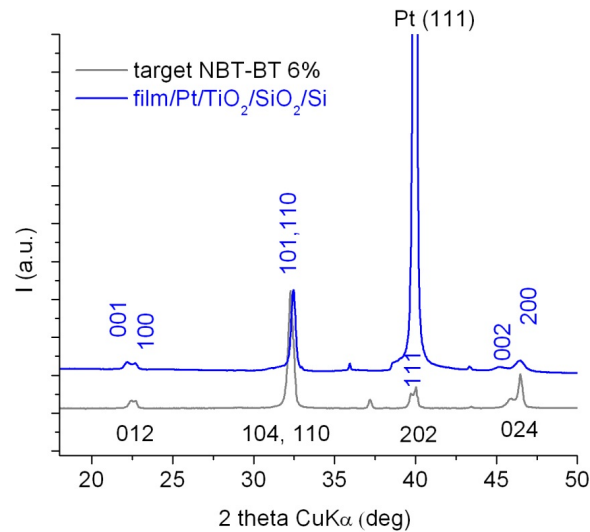
**Figure 6.** XRD spectra of NBT-BT6% deposited on Pt/TiO$_2$/SiO$_2$/Si substrate. The bottom pattern corresponds to the target

Figure 7 displays the XRD patterns of NBT-BT6 films deposited at two temperatures, 650 $^0$C and 700 $^0$C, around the (100)/(001) and (200)/(002) reflections of the Nb:STO substrate. The spectra indicate the epitaxial growth of NBT-BT6% films on the Nb:STO substrate at the two temperatures. This feature is congruent with the microstructure shown in the previous section (Fig. 2 and Fig. 3), consisting of large platelet-like crystallites which preserve the same axis of orientation with the monocrystalline substrate.
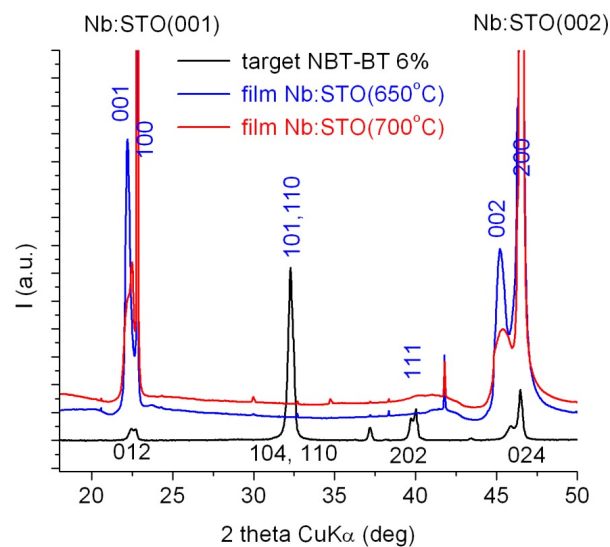


**Figure 7.** XRD spectra of NBT-BT6% /Nb:STONb:STO films deposited at 650 $^o$C and 700 $^o$C. The grey pattern represents the Nb:STONb:STO target reflection peaks.

Figure 8 shows the XRD patterns of NBT-BT8 films grown on Pt/TiO$_2$/SiO$_2$/Si and Nb:STO substrates at 700 $^0$C. The grey pattern represents the NBT-BT8 target spectrum, which corresponds to the tetragonal P4mm symmetry. It can be observed that, similar to the previous composition, the growth on single crystal Nb:STO substrate produces an epitaxial film, while the growth on Pt/TiO$_2$/SiO$_2$/Si substrate results into a polycrystalline randomly oriented film.
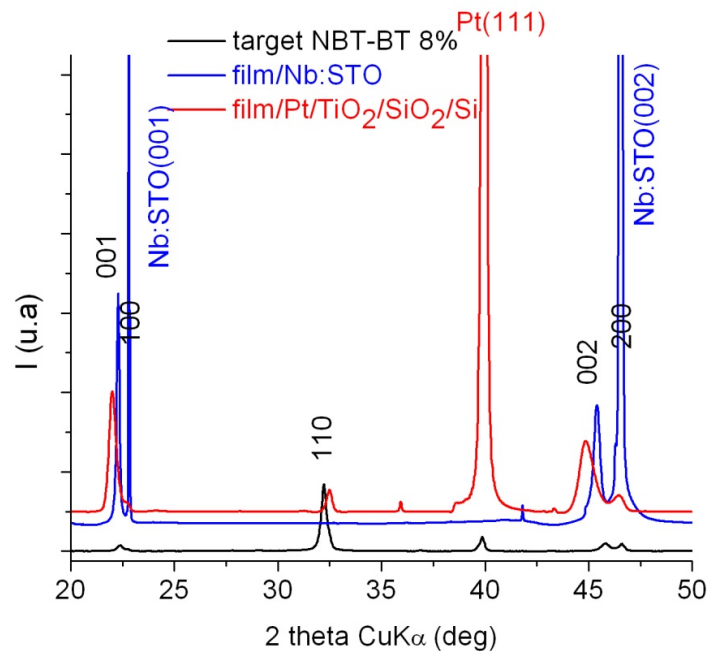


**Figure 8.** XRD spectra of NBT-BT8% deposited on Pt/TiO$_2$/SiO$_2$/Si and on Nb:STONb:STO substrates

### 3.3. Dielectric and ferroelectric properties

The dielectric and ferroelectric properties of NBT-BT thin films have been evaluated on capacitors formed by evaporating through a mask an array of gold electrode dots with an area of about 0.22 mm$^2$ on the surface of films grown on Pt/TiO$_2$/SiO$_2$/Si and Nb:STO substrates. The bottom electrode was formed by the Pt layer in the first case or by the Nb:STO substrate itself in the second case.

The piezoresponce force microscopy results are presented in Figure 9. The full-Pt tips were brought in contact with the surface of the sample and then a *dc* bias and test *ac* bias were applied between the tip and the bottom electrode of the samples. The *dc* bias was generated by a high voltage amplifier and the *ac* bias was generated by a lock-in amplifier. The same lock-in amplifier was used to analyse the vertical deflection signal from the PSPD, in order to extract the amplitude and the phase of the cantilever oscillations induced by the local de-

formation of the sample due to the applied *dc* bias. The NBT-BT6/Pt/Si thin films show good switching behavior, the piezoelectric hysteresis and pronounced imprint (not showed here) confirming the piezoelectric and ferroelectric characteristics. The dependence of effective piezoelectric coefficient $d_{33}$ $^{eff}$ on the applied electric field is given in Figure 9. The locally measured values with the highest being around $d_{33}$ $^{eff}\approx$ 83 pm/V, are even higher then for previouslly reported values for pure NBT or lead-based thin films, such as Pb(ZrTi)O$_3$ or PbTiO$_3$ [21, 22]. However, these $d_{33}$ $^{eff}$ are a bit smaller then NBT-BT6 ceramics which are reported to be more than 100 pm/V [21]. The reasons for these smaller values are related with the film's porosity, but also with the clamping effect which occurs because the PFM tip- applied electric field will piezoelectrically deform only a small fraction of the film. The rest of the sample will restrict the relative deformation of this small fraction, resulting a lower value for $d_{33}$ $^{eff}$ [5, 22].
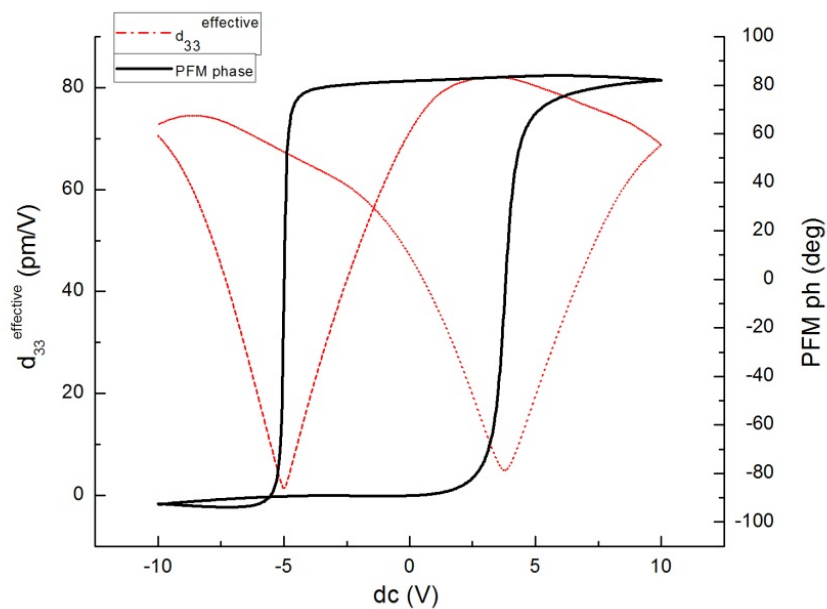


**Figure 9.** The piezoresponse measurements performed on NBT-BT6 thin films.

In Fig. 10 the room temperature dielectric properties of NBT-BT6 films deposited on Pt/ TiO$_2$/SiO$_2$/Si at different substrate temperatures, 650 $^0$C and 730 $^0$C, have been compared in the frequency range 100 Hz-1 MHz. Films grown at 650 $^0$C show a higher dielectric constant ($\varepsilon'$ ~ 1000), in the order of magnitude of the bulk values ($\varepsilon'_{bulk}$ ~ 1900), while films grown at 730 $^0$C show lower values ($\varepsilon'$ ~ 700). The dielectric loss values are instead comparable in the two samples, and similar to bulk values.
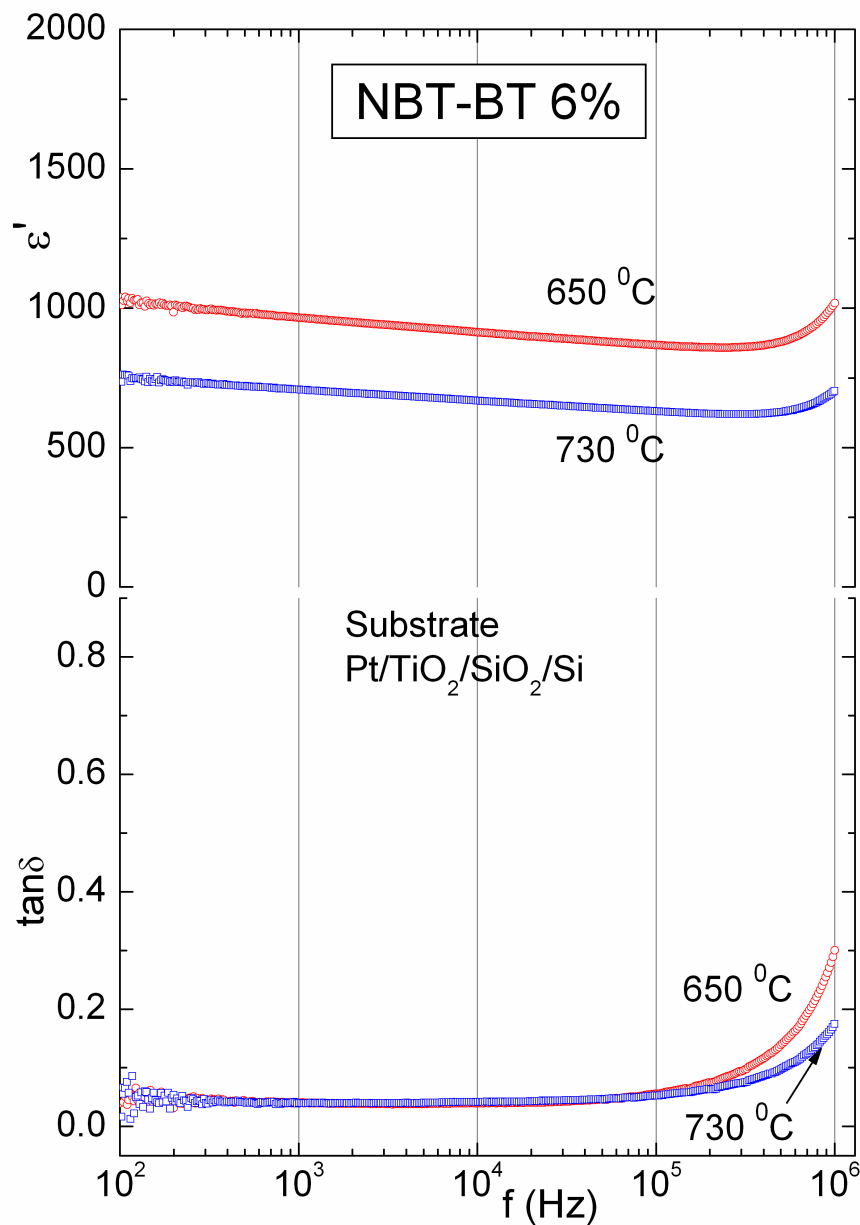
**Figure 10.** Room temperature dielectric constant ε' and loss tanδ variation with frequency for NBT-BT6% films deposited at different temperatures on Pt/TiO₂/SiO₂/Si.

Figure 11 displays the room temperature dielectric constant and dielectric loss in the frequency range 100 Hz-1 MHz for NBT-BT8 films grown on Pt/TiO₂/SiO₂/Si at different temperatures: 650, 700 and 730 ⁰C. Unlike the previous composition, in this case growth at higher substrate temperatures was beneficial for the improvement of dielectric properties, at least in the frequency domain up to a few hundred kHz. Above this frequency there is a strong increase of dielectric loss. Since an increase is registered also in the dielectric constant, this could be caused by a relaxation mechanism which is active at room temperature at these frequencies, like e.g. free charge relaxation.
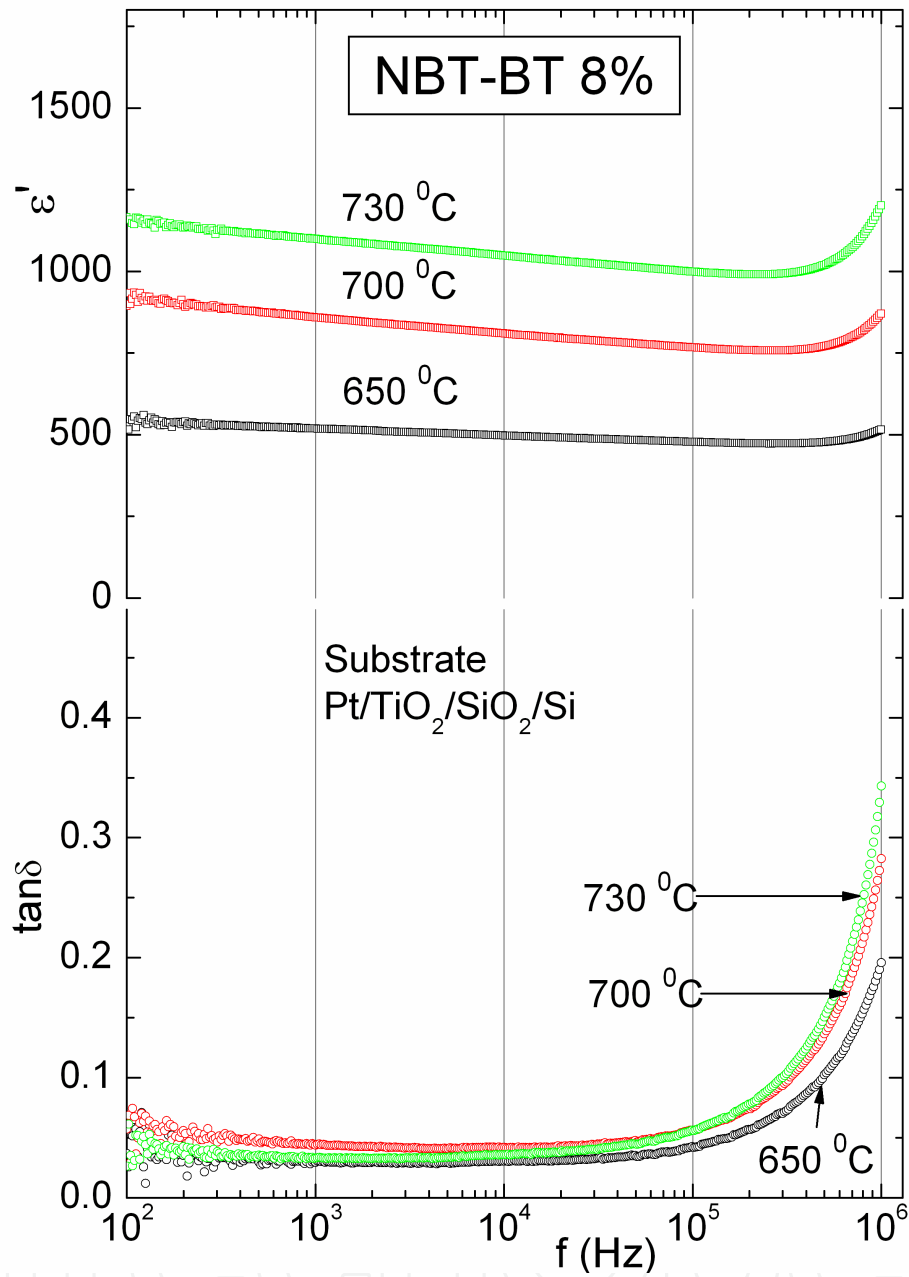
**Figure 11.** Room temperature dielectric constant and loss variation with frequency for NBT-BT8% films deposited at different temperatures on Pt/TiO$_2$/SiO$_2$/Si

Polarization hysteresis measurements on NBT-BT6 films grown on Pt/TiO$_2$/SiO$_2$/Si are shown in Fig. 12. Spontaneous polarization was about 30 μC/cm$^2$ and the remnant polarization was about 10 μC/cm$^2$. The rather high value of coercive field (100 kV/cm) could be explained by the presence of intrinsic strain and pinning defects.

Dielectric and ferroelectric properties measurements on films deposited on Nb:STO substrates have been less reliable, probably due to the presence of a non-ohmic contact at the NBT-BT film – semiconductor Nb:STO interface. However PFM measurements (not shown

here) evidenced good piezoelectric response, which indicates good intrinsic dielectric and ferroelectric properties, although quantitative values are difficult to extract.
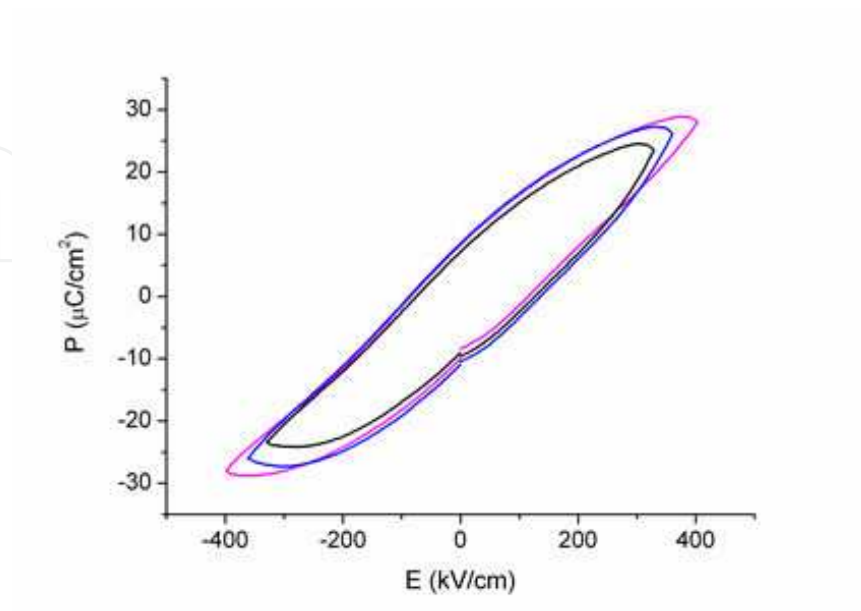


**Figure 12.** Polarization-electric field hysteresis loop measured on a NBT-BT6% film deposited on Pt/TiO$_2$/SiO$_2$/Si

### 3.4. Phase transitions

Phase transitions in ferroelectric materials are accompanied by anomalies of complex dielectric permittivity variation with temperature, generally narrow peaks or steps, depending on the type of phase transformation. However NBT-BT compositions near the morphotropic phase boundary behave as relaxors, due to the cation disorder. This is evidenced in Fig. 13 for NBT-BT8 bulk material. The main characteristic of a relaxor ferroelectric is a broad dielectric peak at a temperature $T_m$ which is not related to a structural transformation. This is due to a wide distribution of relaxation times which characterizes the dielectric response of polar nanoregions. This peak shifts with the increasing of the measurement frequency toward higher temperatures. Thus the dielectric maximum of NBT-BT8 shifts from about 497 K at 200 Hz to about 512 K at 100 kHz. A similar dependence is obeyed also by the dielectric loss.

In Fig. 14 the variation of dielectric constant and loss with temperature for a NBT-BT8 film deposited on Pt/TiO$_2$/SiO$_2$/Si is shown. The maximum of the dielectric constant occurs at about 485 K, not far from bulk $T_m$. However the anomaly is characteristic of a well-behaved phase transition, since the peak temperature $T_m$ does not shift with frequency. A similar qualitative behavior was observed also on the dielectric permittivity variation with temperature for NBT-BT6 films (not shown here).
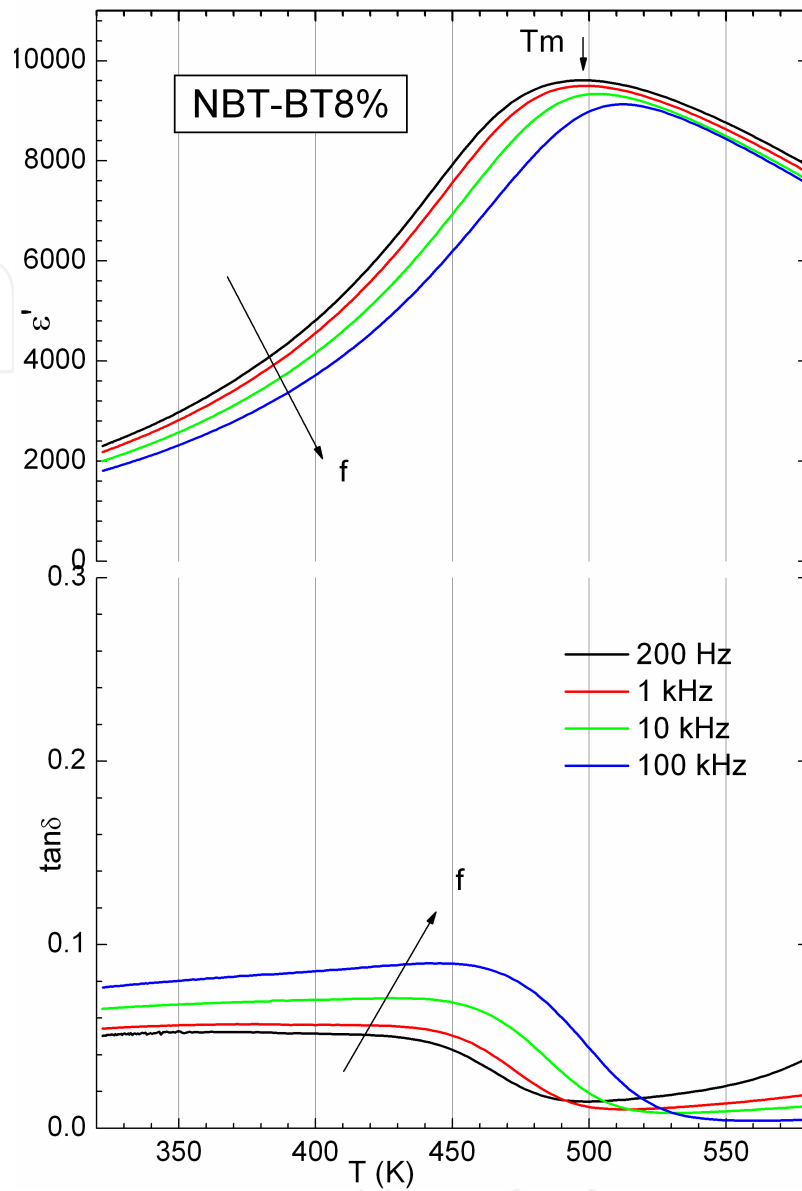
**Figure 13.** The dielectric permittivity and loss variation with temperature measured on a NBT-BT8% bulk sample at different frequencies. The long arrows mark the increasing of frequency.

While the dielectric permittivity peak position Tm ~ 485 K does not shift with measuring frequency, peak height is strongly dependent on it, decreasing for higher frequencies. This can be attributed to the possible presence of a non-polar dielectric layer, which does not influence the general behavior at phase transition, but can modify the value of the dielectric constant [23]. Generally these interface layers can have strong frequency-dependent dielectric properties which influence the overall properties of the heterostructures. However we stress again that the dependence on temperature and phase transition temperatures can be influenced only in the limits of a monotonous contribution, since the dielectric behaviour of non-polar layers is free of temperature anomalies. Indeed the stronger variation with

temperature of the peak intensity at $T_m$ could be attributed to the non-polar layer contribution at higher temperatures due to conductivity variation.

The temperature Td where a strong increase of dielectric loss and dielectric constant occurs marks the ferroelectric – antiferroelectric phase transition which, in bulk samples with the same composition is visible only in the poled state. It is called also depolarization temperature.
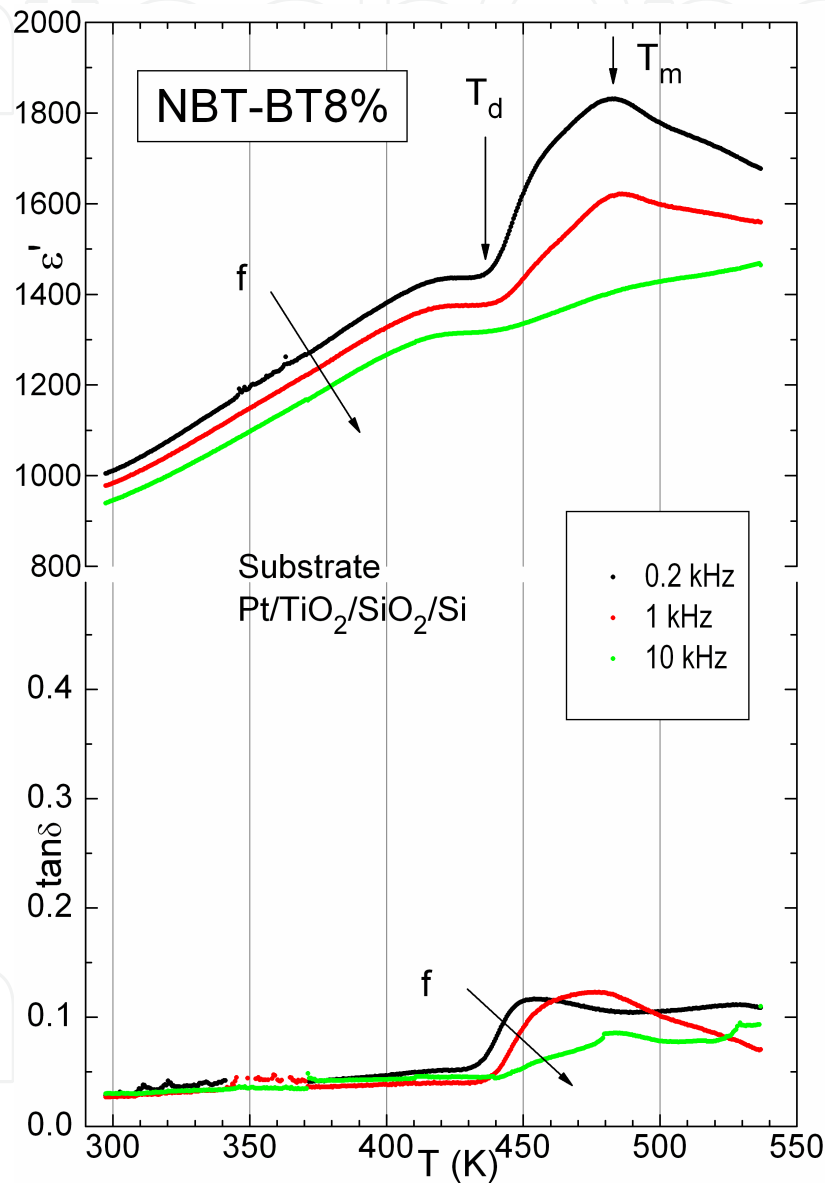


**Figure 14.** The dielectric permittivity and loss variation with temperature measured on a NBT-BT8% thin film at different frequencies. The long arrows mark the increasing of frequency.

An apparent frequency dependence of the step increase in tanδ which marks $T_d$ is visible on the lower curves in Fig. 14. This could be attributed to a partial relaxor behavior due to mixed nanodomains-normal ferroelectric domains, which can be find also, but in proportion displaced to the nanodomain limit, in bulk samples. We must remark that the films were not

poled, since no bias electric field was applied. Therefore the occurrence of a ferroelectric ground state in the NBT-BT films, in striking contrast with relaxor bulk samples with the same composition, must be generated by some intrinsic differences between ceramic bulk samples and ceramic thin films. The first and most obvious reason could be related to the constraining stress of the substrate on the thin films. This is strong in epitaxially grown thin films with a thickness generally below 100 nm, but it should be almost absent in polycrystalline films, randomly oriented and with a thickness of several hundreds of nm. This last one is the case for NBT-BT thin films deposited on $Pt/TiO_2/SiO_2/Si$ substrates. The second reason could be related to the strong differences in the microstructures of ceramic thin films and bulk materials with the same composition. Therefore the occurrence of a ferroelectric ground state instead of a relaxor state in NBT-BT films, as well as the occurrence of a true ferroelectric phase transition could be due to the constrainig imposed by the nanograin boundaries on the ensemble of polar nanoregions.

## 4. Conclusions

In summary, we have investigated the role of deposition temperature and substrate type as well as the amount of BT present in the target on crystalline structure, microstructure, dielectric properties, phase transition temperatures and stability limits of ferroelectric phases in NBT-BT thin films grown by pulsed laser deposition. We have successfully deposited pure perovskite epitaxial films on single-crystal Nb:STO substrates. Successful growth of NBT-BT films on platinized silicon substrates has been achieved. Good dielectric and ferroelectric properties, comparable with bulk values, have been obtained. The NBT-BT6/Pt/Si thin films show a classic switching behavior, the piezoelectric hysteresis and pronounced imprint confirming the piezoelectric and ferroelectric characteristics. The locally measured value of effective piezoeletric coefficient $d_{33}^{\,eff}$ was around 83 pm/V, higher to the previouslly reported values for pure NBT or lead-based thin films. An enhanced stability of ferroelectric phase in thin films with respect to bulk has been observed and explained by their peculiar nanocrystalline microstructure.

## Author details

N. D. Scarisoreanu[1*], R. Birjega[1], A. Andrei[1], M. Dinescu[1], F. Craciun[2] and C. Galassi[3]

*Address all correspondence to: snae@nipne.ro

1 NILPRP, National Institute for Laser, Plasma & Radiation Physics, Bucharest, Romania

2 CNR-ISC, Istituto dei Sistemi Complessi, Area della Ricerca Roma-Tor Vergata, Roma, Italy

3 CNR-ISTEC, Istituto di Scienza e Tecnologia dei Materiali Ceramici, Faenza, Italy

# References

[1] Saito, Y., Takao, H., Tani, T., Nonoyama, T., Takatori, K., Homma, T., Nagaya, T., & Nakamura, M. (2004). Lead-free piezoceramics. *Nature*, 432, 84.

[2] Smolenski, G. A., Isupov, V. A., Agranovskaya, A. I., & Krainik, N. N. (1961). New ferroelectrics of complex composition, Sov. *Phys. Solid State*, 2, 2651-196.

[3] Chiang, Y. M., Farrey, G. W., & Soukhojak, A. N. (1998). Lead-free high-strain single-crystal piezoelectrics in the alkaline-bismuth-titanate perovskite family. *Appl. Phys. Lett*, 73, 3683.

[4] Takenaka, T., & Nagata, H. (1999). Present Status of Non-Lead-Based Piezoelectric-Ceramics. *Key Engineering Materials*, 157/158, 57.

[5] Takenaka, T, Maruyama, K.-I., & Sakata, K. (1991). (Bi1/2Na1/2)TiO3-BaTiO3 System for Lead-Free Piezoelectric Ceramics. *Jpn. J. Appl. Phys*, 30, 2236-2239.

[6] Jones, G. O., & Thomas, P. A. (2002). Investigation of the structure and phase transitions in the novel A-site substituted distorted perovskite compound Na0.5Bi0.5TiO3, Acta Crystallogr. *Sect. B: Struct. Sci*, 58, 168 -178 .

[7] Hiruma, Y., Watanabe, Y., Nagata, H., & Takenaka, T. (2007). Phase Transition Temperatures of Divalent and Trivalent Ions Substituted (Bi1/2Na1/2)TiO3 Ceramics, Key Eng. *Mater*, 350, 93.

[8] Glazer, A. M. (1972). The classification of tilted octahedra in perovskites, Acta Crystallogr. *Sect. B: Struct. Sci*, 28, 3384.

[9] W.-van, B., Eerd, D., Damjanovic, N., Klein, N., Setter, , & Trodhal, J. (2010). Structural complexity of (Na0.5Bi0.5)TiOP3BaTiO3 as revealed by Raman spectroscopy. *Phys. Rev. B*, 82, 104112.

[10] Ma, C., & Tan, X. (2010). Phase diagram of unpoled lead-free (1-x)(Bi/sub 1/2/Na/sub 1/2/)TiO/sub 3-x/BaTiO/sub 3/ ceramics. *Solid State Commun*, 150, 1497-1500.

[11] Cordero, F., Craciun, F., Trequattrini, F., Mercadelli, E., & Galassi, C. (2010). Phase transitions and phase diagram of the ferroelectric perovskite (Na0.5Bi0.5)1−xBaxTiO3 by anelastic and dielectric measurements. *Phys. Rev. B*, 81, 144124.

[12] Guo, Y. P., Akai, D. S., Sawada, K., & Ishida, M. (2008). Dielectric and ferroelectric properties of highly (100)-oriented (Na0.5Bi0.5)0.94Ba0.06TiO3 thin films grown on LaNiO3/γ-Al2O3/Si substrates by chemical solution deposition. *Solid State Sciences*, 10, 929.

[13] Guo, Y. P., Akai, D. S., Sawada, K., Ishida, M., & Gu, M. Y. (2009). Structure and electrical properties of trilayered BaTiO3/(Na0.5Bi0.5)TiO3BaTiO3/BaTiO3 thin films deposited on Si substrate. *Solid State Communications*, 149, 14.

[14] Duclère, J.R., Cibert, C., Boulle, A., Dorcet, V., Marchet, P., Champeaux, C., Catherinot, A., Députier, S., & Guilloux-Viry, M. (2008). Lead-free Na0.5Bi0.5TiO3 ferroelec-

tric thin films grown by Pulsed Laser Deposition on epitaxial platinum bottom electrodes. *Thin Solid Films*, 517, 592.

[15]  Bousquet, M., , J., Ducle`re, R., Gautier, B., Boulle, A., Wu, A., De´, S., putier, D., Fasquelle, F., Re´mondie`, re. D., Albertini, C., Champeaux, P., Marchet, M., Guilloux- , Viry, & Vilarinho, P. (2012). Electrical properties of (110) epitaxial lead-free ferroelectric Na0.5Bi0.5TiO3 thin films grown by pulsed laser deposition: Macroscopic and nanoscale data. *J. Appl. Phys*, 111, 104 -106.

[16]  Qin, W., Guo, Y., Guo, B., & Gu, M. (2012). Dielectric and optical properties of BiFeO3-(Na0.5Bi0.5)TiO3 thin films deposited on Si substrate using LaNiO3 as buffer layer for photovoltaic devices. *J. Alloys Compd*, 513, 154-158.

[17]  Shaw, T. M., Trolier Mc Kinstry, S., & Mc Intyre, P. C. (2000). The properties of ferroelectric thin films at small dimensions. *Annu. Rev. Mater. Sci*, 30, 263.

[18]  Scarisoreanu, N., Craciun, F., Chis, A., Birjega, R., Moldovan, A., Galassi, C., & Dinescu, M. (2010). Lead-free ferroelectric thin films obtained by pulsed laser deposition. *Appl. Phys A*, 101, 747 -751 .

[19]  Scarisoreanu, N., Craciun, F., Ion, V., Birjega, S., & Dinescu, M. (2007). Structural and electrical characterization of lead-free ferroelectric Na/sub 1/2/Bi/sub 1/2/TiO/sub 3/-BaTiO/sub 3/ thin films obtained by PLD and RF-PLD. *Appl. Surf. Sci*, 254, 1292.

[20]  Picht, G., Töpfer, J., & Henning, E. (2010). Structural properties of (Bi0.5Na0.5)1−xBaxTiO3 lead-free piezoelectric ceramics. *J. Eur. Ceram. Soc*, 30, 3445.

[21]  Takenaka, T. (1999). Piezoelectric Properties of Some Lead-Free Ferroelectric Ceramics. *Ferroelectrics*, 230, 87-98.

[22]  Morelli, A., Sriram, Venkatesan, Palasantzas, , Palasantzas, Kooi, G, & De Hosson, J. Th. M. (2009). Piezoelectric properties of PbTiO3 thin films characterized with piezoresponse force and high resolution transmission electron microscopy. *J. Appl. Phys*, 105, 064106.

[23]  Craciun, F., & Dinescu, M. (2007). Piezoelectrics", in "Pulsed laser deposition of thin films: applications-led growth of functional materials". *edited by R. Eason (Wiley-Interscience, John Wiley & Sons, Hoboken, New Jersey, U.S.A.,)*, 487-532.